Microstructure and Self-Assembly of Inhomogeneous Rigid Rodlike Chains between Two Neutral Surfaces: A Hybrid Density Functional Approach

Dapeng Cao,* Menghan Zhu, and Wenchuan Wang

Lab of Molecular and Materials Simulation, College of Chemical Engineering, Beijing University of Chemical Technology, Beijing 100029, P. R. China

Received: June 28, 2006; In Final Form: August 21, 2006

We use a hybrid density functional approach to investigate the microstructure and self-assembly of inhomogeneous rigid rodlike chains between two neutral surfaces, i.e., two hard walls. In the calculation, the rodlike molecule is modeled as a rigid rod linearly connected by the tangent sphere beads. The hybrid method combines a single-chain Monte Carlo (MC) simulation for the ideal-gas part of Helmholtz energy and a DFT approach for the excess Helmholtz energy. The DFT approach includes a modified fundamental measure theory for the excluded-volume effect, the first order thermodynamics perturbation theory for chain connectivity, and the mean field approximation for the van der Waals attraction. We investigate the effect of the chain length (i.e., aspect ratio) of the rodlike molecule and the separation between two surfaces on the microstructure and self-assembly of inhomogeneous rigid rodlike chains. For the athermal systems, the rodlike chain fluids present a smaller partitioning coefficient compared to the flexible chain fluids. For the thermal systems, lamellar thin films formed by the rigid rodlike molecules perpendicular to the neutral surface are observed. The effects of the head−head interaction and the separation on the self-assembly of the rodlike chain fluids in the slit are investigated.

1. Introduction

Since Onsager predicted that the hard spherocylindrical fluids could undergo a nematic (N)−isotropic (I) phase transition,[1] a lot of simulation,[2] experimental,[3] and theoretical investigations[4] have been performed. These investigations were mainly focused on the phase boundaries of isotropic (I), nematic (N), and smectic-A regions and the phase transition of hard spherocylindrical and rodlike chain fluids,[3−7] because the rodlike chain also has the analogic structure with the spherocylinder. The spherocylindrical and rigid rodlike molecules are often used as a model to represent liquid crystals. Therefore, understanding the properties of inhomogeneous spherocylindrical or rodlike chain fluids near a surface is important for the design of substrate based devices, such as the ordered lamellar thin films. In addition, the hard rodlike or spherocylindrical fluids also often act as a shield to stabilize a solution or as an additive to induce the colloids into self-assembly,[8−12] which are similar to the properties of a flexible polymeric stabilizer.[13]

On the basis of the density functional theory (DFT) proposed by Somoza and Tarazona, Velasco et al.[14] calculated the smectic phase boundaries for the hard spherocylindrical fluids. In their work, the calculations were only performed for the bulk phase. Recently, de las Heras et al.[15] extended the standard Onsager-type DFT to spatially inhomogeneous phases to examine the wetting properties of the hard spherocylinder against a selective surface. In their results, the magnitude of nematic order changes with the different preference of the surface.

Using the needle model to represent the rod and the hard sphere model to represent colloids, Schmidt[10] calculated the rod−colloid binary mixtures by the density functional theory by combining Rosenfeld's fundamental measures theory and the Tarazona latest extension.[16] Then, Bryk[8] calculated the rod−polymer mixtures by connecting the functional from Yu and Wu for polymer mixtures[17] and Schmidt's functional for rod-sphere mixtures. They found that the addition of rodlike fluids causes the aggregation of colloids or polymers due to the depletion effect at low volume fractions. Additionally, Vega et al.[18,19] investigated the liquid crystal phase formation of the rodlike chain (also called linear tangent hard sphere chain) fluids by using Monte Carlo simulation, and found that the critical length of the aspect ratio for the smectic-A phase is $M = 5$, rather than $M = 6$ proposed by Flory lattice theory, where M is the number of atoms of a chain molecule. Furthermore, they also explored an equation of state for the rodlike chain fluids[20] and the effect of the intramolecular flexibility on the isotropic−nematic phase transition of the fused hard sphere chain.[6]

For the spherocylindrical fluids, to our knowledge, only de las Heras et al.[15] investigated the properties of spherocylindrical fluids near the surface using the theoretical method. For the rodlike chain fluids,[21−23] Cao et al.[21] explored the formation of a nematic monolayer by rigid rodlike molecules standing perpendicular to a planar surface. van Roij et al.[22] investigated the continuous surface phase transition from uniaxial to biaxial local symmetry. However, for flexible chain fluids, Sokolowski and coauthors[24−26] explored the wetting and layering transition and capillary condensation in detail. Obviously, the microstructure of the rodlike chain fluids is distinctly different from that of flexible chains. The rodlike molecules can form the nematic order structure against the strongly preferential surfaces,[21] while the flexible chains only undergo the layer transition without any nematic order structure near the strongly selective surface.[25] It may be because the flexible chain can freely fill up the surface

* Address correspondence to this author. E-mail: cao_dp@hotmail.com and caodp@mail.buct.edu.cn.

10.1021/jp064040m CCC: $33.50
Published on Web 09/29/2006

but the rigid rod must keep the stiff molecular structure and the arrangement in a specific orientation.

It is worth noting that Kierlik and Roseinberg[27] pointed out the fact that in association-based DFT, the excess part of the free-energy functional depends only on the segment densities without consideration of molecular orientation. Therefore, they believed that the association-based DFT cannot account for a bulk isotropic−nematic phase transition. In contrast, the DFT methods used in the literature,[14,15,22,28,29] which take into account the molecular orientation, can be applied to calculations of the bulk isotropic−nematic phase transition. However, it should be pointed out that although the orientational correlations are absent in the excess free energy of the association-based DFT, the DFT can still yield reasonable results for the segment densities and also some information of orientational structure,[21] because the molecular orientation incarnated in the ideal part of the Helmholtz energy can be reflected in the segment densities.

Since the DFT method based on the modified fundamental measure theory (MFMT) was proposed,[30,31] it has been extensively applied to properties of different polymeric systems, including the microstructures of flexible polymeric fluids,[17,32−34] surface forces between polymer brushes,[35] and adsorption of polymer fluids in model pores.[25,26,36,37] All these investigations indicate that the DFT is not only fairly suitable for the polymeric fluids, but also very accurate in numerical calculations compared to the simulation data. Furthermore, in our previous publication,[21] we have observed the nematic order structure of the rodlike molecules perpendicular to a strongly attractive surface. Obviously, the formation of the nematic order structure is attributed to the attraction of the surface. If the attraction of the surface is removed, the microstructure of the rodlike chain fluids near the neutral surface would change. For example, at low volume fractions, no depletion effect appears for the attractive surface, while the depletion effect occurs for the neutral surface. Accordingly, here we intend to investigate the microstructures of athermal rodlike chain fluids and the self-assembly of thermal rodlike chain fluids confined between two neutral surfaces systematically.

The remainder of this paper is organized as follows. First, we briefly depict the hybrid method combining the single chain simulation for the ideal part of the Helmholtz energy functional and the DFT for the excess part of the Helmholtz energy functional. Second, we present a molecular model for the rigid rodlike molecule based on the coarse-grained means. Then, we investigate the microstructures of the athermal systems containing hard rodlike chains and the self-assembly of the thermal systems containing the attractive rodlike chains confined between two neutral surfaces, i.e., two hard walls. Finally, some significant discussion is addressed.

2. A Hybrid Density Functional Theory

2.1. Helmholtz Energy Functional. The Helmholtz energy functional $F[\rho_M(\mathbf{R})]$ is conventionally expressed as an ideal contribution corresponding to the system of ideal chains that interact only through bonding potentials and an excess part taking into account the contributions from nonbonded chain connectivity interaction, hard sphere repulsion effect, and short-ranged van der Waals attraction, given by[38]

$$F[\rho_M(\mathbf{R})] = F_{id}[\rho_M(\mathbf{R})] + F_{ex}[\rho(\mathbf{r})] \tag{1}$$

where $\rho_M(\mathbf{R})$ is a multidimensional density profile, and $\mathbf{R}$ is a composite vector $(\mathbf{r}_1,\mathbf{r}_2, ..., \mathbf{r}_M)$ representing the positions of all segments of the polymeric molecule. Subscript M indicates the number of atoms of a chain molecule. The molecular density profile $\rho_M(\mathbf{R})$ is related to the segmental densities by

$$\rho(\mathbf{r}) = \sum_{i=1}^{M} \rho_{si}(\mathbf{r}) = \sum_{i=1}^{M} \int d\mathbf{R}\, \delta(\mathbf{r} - \mathbf{r}_i)\rho_M(\mathbf{R}) \tag{2}$$

where $\rho(\mathbf{r})$ is the total segmental density and $\rho_{si}(\mathbf{r})$ is the local density of segment i. $d\mathbf{R}$ stands for a set of differential volumes $(d\mathbf{r}_1, d\mathbf{r}_2, ..., d\mathbf{r}_M)$.

For the ideal polymer system with only bonding potentials, the Helmholtz energy is known exactly

$$\beta F_{id}[\rho_M(\mathbf{R})] = \int d\mathbf{R}\, \rho_M(\mathbf{R})[\ln \rho_M(\mathbf{R}) - 1] + \beta \int d\mathbf{R}\, \rho_M(\mathbf{R})\, V_B(\mathbf{R}) \tag{3}$$

where the $V_B(\mathbf{R})$ is the direct bond potential $\beta = (kT)^{-1}$, with k being Boltzmann constant and T for temperature

The excess part of the Helmholtz energy functional can be mathematically expressed as

$$\beta F_{ex}[\rho(\mathbf{r})] = \beta F_{ex}^{hs} + \beta F_{ex}^{chain} + \beta F_{ex}^{att} \tag{4}$$

Following our previous work for polymers,[38−40] the hard-sphere part of the Helmholtz energy functional is represented by a modified fundamental measure theory[30,31]

$$\beta F_{hs} = \int d\mathbf{r}\left\{-n_0 \ln(1 - n_3) + \frac{n_1 n_2 - \mathbf{n}_{V1}\cdot\mathbf{n}_{V2}}{1 - n_3} + (n_2^3/3 - n_2 \mathbf{n}_V 2\cdot n_{V2})\left[\frac{\ln(1 - n_3)}{12\pi n_3^2} + \frac{1}{12\pi n_3 (1 - n_3)^2}\right]\right\} \tag{5}$$

where $\nu\alpha(\rho)$ with $\alpha = 0, 1, 2, 3, V1$, and $V2$ are weighted densities defined by Rosenfeld.[41] These scalar and vector weighted densities are given by

$$n_\alpha(\mathbf{r}) = \sum_j n_{\alpha j}(\mathbf{r}) = \sum_j \int \rho_j(\mathbf{r}')\omega_j^\alpha(\mathbf{r} - \mathbf{r}')\, d\mathbf{r}' \tag{6}$$

where ϖ_j^α with $\alpha = 0, 1, 2, 3, V1$, and $V2$ are six weight functions.[42]

The excess Helmholtz energy functional due to the chain connectivity is given by a generalized first-order perturbation theory[38]

$$\beta F_{chain} = \int d\mathbf{r} \frac{1 - M}{M} n_0 \cdot \xi \cdot \ln y^{hs}(\sigma, n_\alpha) \tag{7}$$

where $\xi = 1 - \mathbf{n}_{V2}\cdot\mathbf{n}_{V2}/n_2^2$ is defined as an inhomogeneous factor, M is the number of atoms of a chain molecule, and $y^{hs}(\sigma,n_\alpha)$ is the contact value of the cavity correlation function between segments

$$y^{hs}(\sigma, n_\alpha) = \frac{1}{1 - n_3} + \frac{n_2 \xi \sigma}{4(1 - n_3)^2} + \frac{n_2^2 \xi \sigma}{72(1 - n_3)^3} \tag{8}$$

Equation 7 is not directly related to the bonding potentials of polymeric molecules that have been already included in eq 3. This term takes into account the effect of chain connectivity on the nonbonded interactions between polymeric segments.

Finally, the excess Helmholtz energy functional due to van der Waals attraction, βF_{ex}^{att}, is represented by a mean-field approximation[39]

$$\beta F_{ex}^{att} = \frac{1}{2}\int\int d\mathbf{r}\, d\mathbf{r}' \sum_{i,j=A,B} \rho_i(\mathbf{r})\, \rho_j(\mathbf{r})\, \beta\varphi_{ij}^{att}(|\mathbf{r}-\mathbf{r}'|) \quad (9)$$

where $\varphi_{ij}^{att}(r)$ is described in eq 18.

The main idea of a density functional theory is that given a grand potential functional $\Omega[\rho_M(\mathbf{R})]$, the equilibrium density profile, $\rho_M(\mathbf{R})$, can be solved from the stationary condition[39]

$$\frac{\delta\Omega[\rho_M(\mathbf{R})]}{\delta\rho_M(\mathbf{R})} = 0 \quad (10)$$

thereby all thermodynamic properties can be evaluated following statistical thermodynamic relations. For a polymeric fluid, the grand potential is related to the Helmholtz energy functional $F[\rho_M(\mathbf{R})]$ via the Legendre transform

$$\Omega[\rho_M(\mathbf{R})] = F[\rho_M(\mathbf{R})] + \int[\psi_M(\mathbf{R}) - \mu_M]\rho_M(\mathbf{R})\, d\mathbf{R} \quad (11)$$

where $\psi_M(\mathbf{R})$ is the external potential exerting on individual segments, and μ_M is the chemical potential of the polymer chain.[38]

2.2. Euler−Lagrange Equation. Minimization of the grand potential with respect to the density profiles, namely, eqs 10 and 11, gives the Euler−Lagrange equation

$$\rho_M(\mathbf{R}) = \exp[\beta\mu_M - \beta V_B(\mathbf{R}) - \beta\sum_{i=1}^{M}\lambda_i(\mathbf{r}_i)] \quad (12)$$

where the self-consistent potential $\lambda_i(\mathbf{r}_i)$ includes the derivative of the excess Helmholtz free energy and the external potential $\varphi_i(\mathbf{r}_i)$

$$\lambda_i(\mathbf{r}_i) = \frac{\delta F_{ex}}{\delta\rho(\mathbf{r}_i)} + \varphi_i(\mathbf{r}_i) \quad (13)$$

Combination of eqs 4, 12, and 13 yields the segmental densities $\rho_{si}(\mathbf{r})$

$$\rho_{si}(\mathbf{r}) = \int d\mathbf{R}\, \delta(\mathbf{r}-\mathbf{r}_i) \exp[\beta\mu_M - \beta V_B(\mathbf{R}) - \beta\sum_{j=1}^{M}\lambda_j(\mathbf{r}_j)] \quad (14)$$

Subsequently, the average segment density of chains is represented by

$$\rho(\mathbf{r}) = \exp(\beta\mu_M)\int d\mathbf{R}\sum_{i=1}^{M}\delta(\mathbf{r}-\mathbf{r}_i) \exp[-\beta V_B(\mathbf{R}) - \beta\sum_{j=1}^{M}\lambda_j(\mathbf{r}_j)] \quad (15)$$

where $\exp[-\beta V_B(\mathbf{R})]$ represents the probability density of an ideal hard rodlike molecule with configuration $\mathbf{R}$.[39] For simplicity, let $P(\mathbf{R}) = \exp[-\beta V_B(\mathbf{R})]$. In the hybrid method, the probability density $P(\mathbf{R})$ can be attained by carrying out a single chain simulation with sufficient conformations filling the whole configurational-space, rather than by the integral of the Dirac delta functions used in the pure DFT approach. Equation 14 can be reformulated as

$$\rho_{si}(\mathbf{r}) = \exp(\beta\mu_M)\int d\mathbf{R}\, \delta(\mathbf{r}-\mathbf{r}_i)\cdot P(\mathbf{R}) \exp[-\beta\sum_{j=1}^{M}\lambda_j(\mathbf{r}_j)] \quad (16)$$

2.3. Numerical Calculation. By the average of lots of configurations from the single chain simulation[21,43] we get

$$\rho_{si}(\mathbf{r}) = \exp(\beta\mu_M)\langle\exp[-\beta\sum_{j=1}^{M}\lambda_j(\mathbf{r}_j)\rangle_{\mathbf{r}=\mathbf{r}_i} \quad (17)$$

where $\langle\ \rangle$ is the average weight of all configurations of the single molecules that are independent of the density profiles and the external fields. In particular, in the calculation of local density of segment i, $\rho_{si}(\mathbf{r})$, the segment i is put in the fixed position, $\mathbf{r}$. Then, the positions (r_j) of the other segments of the given single chain are known. As a result, the self-consistent potentials, $\lambda_j(r_j)$, corresponding to all the positions (r_j, $j = 1, 2, ..., M$) can be used in eq 17 to obtain the results. To efficiently represent the whole configurational space, we use a large number ($\sim 10^5$) of rodlike molecular conformations to calculate the ensemble average of eq 17. Compared to the integral of the Dirac delta functions used in the pure DFT, the hybrid method provides less computational cost, because the direct integral in pure DFT has to bear the asymmetry of left and right recursive functions. The expressions on the left and right recursive functions for the rigid molecule can be referred to in ref 39. Accordingly, the time consumption of the direct integral increases exponentially with the chain length.

In our calculation, the Picard iterative method was used to solve eq 17. The iteration started from the bulk density of the rodlike molecule. After a new density profile was obtained, we would combine the new density and the previous one in an appropriate prescription as a new input. Then, the self-consistent potential was modified by eq 13. Iterations were repeated until the deviation between the old density and the new one was smaller than the scheduled error at all the points.

3. Molecular Models

In this work, the rodlike molecule is modeled as a rigid rod linearly connected by tangent sphere beads. For athermal systems, all the sphere beads are neutral, and the interaction between the beads of two molecules is represented by the hard sphere potential. Accordingly, the rodlike molecule has a hard core repulsion. It is entirely different with the needle model of vanishing thickness, which was extensively used in the work of Schmidt et al.[10] and other researchers.[8,9] Compared to the needle of vanishing thickness, actually, our model with the hard core repulsion is more rational to represent practical rodlike molecules.

For thermal systems, we define the first bead of the rodlike chain as the "head" segment, and the other beads as the "tail" segments. To mimic the rigid surfactant-like molecule, we assume that the like-pair interaction is attractive, and the unlike-pair interaction is immiscible. The pair interaction is represented by square-well potential

$$\varphi_{ij}(r) = \begin{cases} \infty & r < \sigma \\ -\epsilon_{ij} & \sigma \le r \le \gamma\sigma \\ 0 & r > \gamma\sigma \end{cases} \quad (18)$$

where σ is the segment diameter, $\gamma\sigma$ is the square-well width, and ϵ_{ij} is an energy parameter with the indexed segments. Throughout this work, the attractive width is fixed at $\gamma = 1.2$.

4. Results and Discussion

4.1. Athermal Systems. We first consider the athermal systems containing rodlike molecules of different chain lengths, i.e., aspect ratios. Figure 1 shows the microstructure of hard

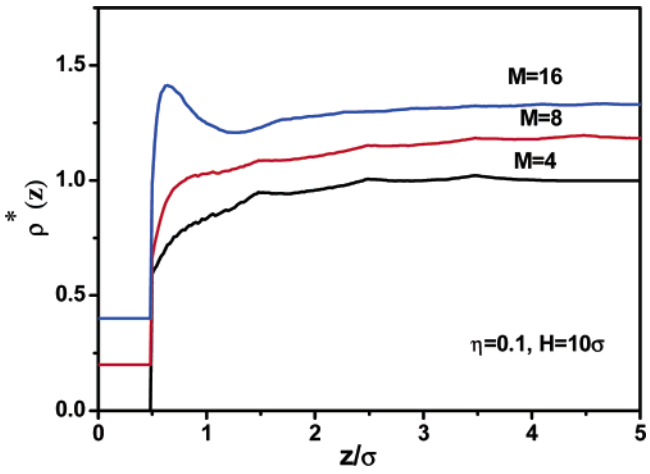

Figure 1. Microstructure of hard rodlike molecules of chain length $M = 4$, 8, and 16 at $\eta = 0.1$ and $H = 10\sigma$. The curves corresponding to $M = 8$ and 16 are shifted upward 0.2 and 0.4, respectively.

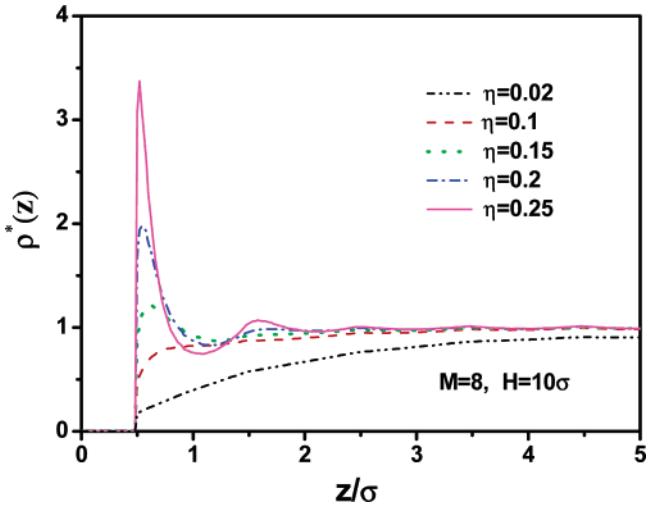

Figure 2. Microstructure of hard rodlike molecules of chain length $M = 8$ at $H = 10\sigma$ and different volume fractions.

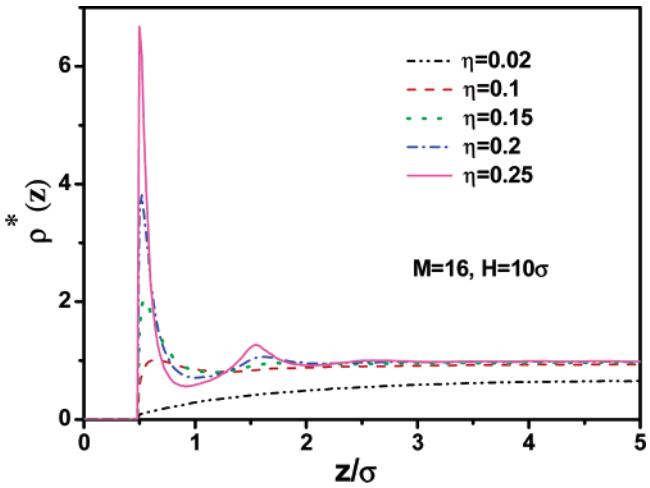

Figure 3. Microstructure of hard rodlike molecules of chain length $M = 16$ at $H = 10\sigma$ and different volume fractions

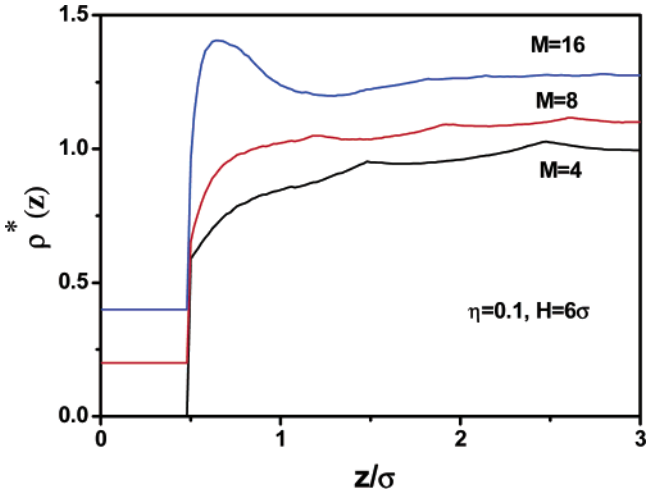

Figure 4. Microstructure of hard rodlike molecules of chain length $M = 4$, 8, and 16 at $\eta = 0.1$ and $H = 6\sigma$. The curves corresponding to $M = 8$ and 16 are shifted upward 0.2 and 0.4, respectively.

rodlike molecules with the chain length $M = 4$, 8, and 16 at the volume fraction $\eta = 0.1$ and $H = 10\sigma$ (σ is the diameter of segments). When the molecular length is smaller than the separation, say, $M = 4$ and 8, the depletion effect is observed near the surface. This is because at low volume fractions, the presence of the surfaces reduces the configurational entropy of the rodlike molecules, causing the local density of the molecules to be smaller than the density of the bulk phase, which is at the same chemical potential as the confined fluid. Interestingly, for the molecule with the length of $M = 16$, which is larger than the separation, the peak of local density arises near the surfaces. In this case, the hard molecules have to adjust their orientations for entering the slit. Furthermore, only the orientations parallel or tilting to the surfaces are validated for entering the slit. Although the loss of the configurational entropy due to the presence of the surfaces would make the decrease of the local density near the surfaces, the packing effect in confinement causes the increase of the local density near the surfaces. In this case, the packing effect in confinement dominates the competition. From the above observation, we find that not only the volume fraction but also the molecular length affects the competition between the depletion and the packing effects.

To get insight into the effect of the bulk volume fraction on the microstructure, we present in Figure 2 the local density profiles of the hard rodlike molecules with chain length $M = 8$ at $H = 10\sigma$ and different volume fractions. At quite low bulk volume fraction $\eta = 0.02$, a strong depletion effect appears. With the increase of the bulk volume fraction, the depletion effect near the surfaces disappears slowly and is gradually replaced by the packing effect, because the packing effect gradually dominates the competition between the configurational entropy and the packing effect. For the molecules of $M = 8$, the local density still presents the depletion effect at $\eta = 0.1$. Furthermore, the peak of the local density near the surfaces at $\eta = 0.25$ is only around 3−4 times the bulk density. However, the molecule of $M = 16$ presents a peak more than 6 times the bulk density at the same condition, implying that the molecular length accelerates the change from depletion effect to packing effect. Figure 3 shows the microstructure of the hard rodlike chains at the same conditions as Figure 2, except that molecular length is $M = 16$. For the high bulk volume fractions, say $\eta = 0.2$ and 0.25, not only the main peak appears near the surface, but also the second peak arises at the position $z = 1.5\sigma$ for both the molecules of $M = 8$ and 16.

To investigate the effect of the separation on the local density of the hard rodlike chains, we present in Figure 4 the microstructure of the hard rodlike chains at the same conditions as in Figure 1 except for the separation of $H = 6\sigma$. For the molecules of $M = 4$, 8, and 16, the local densities of the hard rodlike chains exhibit the same behavior basically as that in

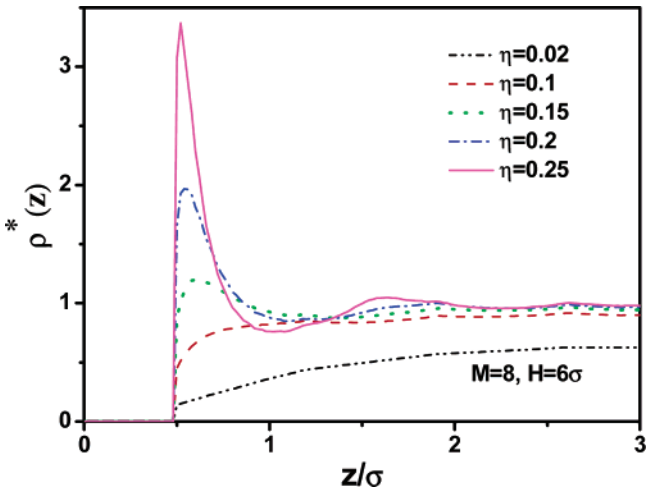

Figure 5. Microstructure of hard rodlike molecules of chain length $M = 8$ at $H = 6\sigma$ and different volume fractions.

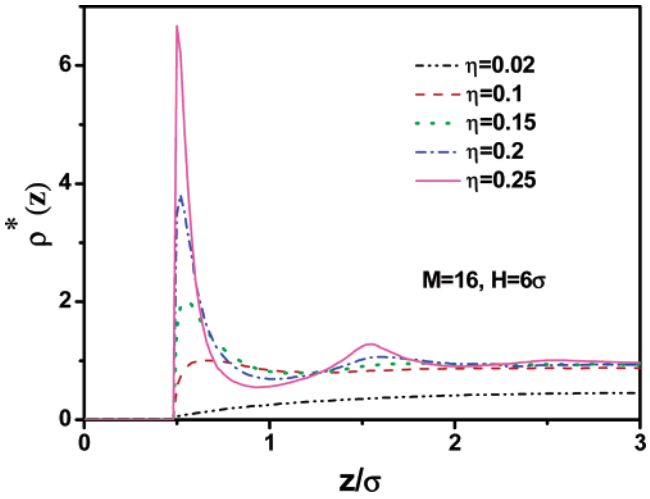

Figure 6. Microstructure of hard rodlike molecules of chain length $M = 16$ at $H = 6\sigma$ and different volume fractions

Figure 1. The only difference is that the local density of the hard rodlike chains of $M = 4$ shows three slight peaks for the separation of $H = 10\sigma$, in contrast to one peak and one shoulder for the separation of $H = 6\sigma$.

In particular, Figure 5 shows the microstructure of the hard rodlike chains at the same conditions as in Figure 2 except for the separation of $H = 6\sigma$. Due to the decrease of the separation, the depletion effect becomes more distinct at the low bulk volume fraction of $\eta = 0.02$, which is described by the lower densities than the bulk at the center of the slit. However, the packing effect remains basically the same intensity for the two separations of $H = 6\sigma$ and 10σ. Figure 6 presents the local density of the hard rodlike chains at the same conditions as in Figure 5 but the molecular length is equal to 16 (i.e., $M = 16$). In this case, the local density at the center of the slit is only a half of the bulk density of $\eta = 0.02$, meaning the extremely strong depletion effect. This observation is rational, because the long rodlike molecule does not like entering the hard slit due to the loss of the configurational entropy.

The partitioning coefficient is often used to represent the difference in the volume fractions between the confined and bulk phases. The partitioning coefficient is defined as

$$K_c = \rho_{pore}^{ave}/\rho_{bulk} \tag{19}$$

Figure 7 presents the partitioning coefficient as a function of bulk volume fraction for hard rodlike chain fluids with the molecular lengths of $M = 8$ and 16. For the low volume fraction $\eta = 0.02$, the partitioning coefficient presents the smallest value at $M = 16$ and $H = 6\sigma$, while it presents the largest at $M = 8$ and $H = 10\sigma$ in these cases studied. This means that the longer the molecular length, the more distinct is the depletion effect at low bulk volume fractions. Similarly, the smaller the separation between two surfaces, the more distinct is the depletion effect. To compare the effect of the stiffness of molecules on partitioning coefficient, the partitioning coefficient of the flexible chain of $M = 8$ at the slit of $H = 5\sigma$ is also presented in Figure 7, denoted by open diamond points. Obviously, in all the bulk densities, the partitioning coefficient of flexible chains is larger than that of the hard rodlike molecules, suggesting that stiffness of the rodlike molecules would reduce the partitioning coefficient. That is to say, it is more difficult for the rodlike chain to enter the slit, compared to flexible chains.

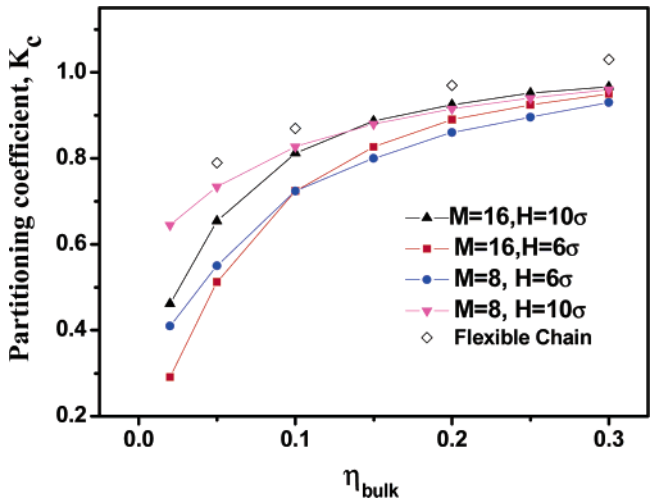

Figure 7. Partitioning coefficient as a function of bulk volume fraction for hard rodlike chain fluids of chain length $M = 8$ and 16.

4.2. Thermal Systems. In this section, we consider the thermal system in which the rodlike molecule comprises head and tail segments. To mimic the rigid surfactant, we define the first segment of the rodlike molecule as the "head", and the other segments as the "tail". The rodlike model provides a simple representation of hydrophobic and hydrophilic components of a rigid surfactant. To gain insight into the self-assembly of the rodlike molecules, we employ the square-well (SW) potential presented in eq 18 to represent the short-ranged attraction between head and head, or tail and tail. To make the hydrophobic and hydrophilic components efficiently into phase separation, a slight repulsion was used to represent the interaction between head and tail segments. In the calculation, the chain length (i.e., aspect ratio) of the rodlike molecule was set to $M = 4$, and the interactions between tails and between head and tail segments were fixed at $\epsilon_{TT}^* = 1$ and $\epsilon_{HT}^* = -1$ (negative stands for the repulsion), respectively. To remove the effect of the surface preference on the self-assembly of the rodlike molecules, we used two neutral surfaces here, i.e., two hard walls. Accordingly, we can separately explore the effect of the head−head interaction on the self-assembly of the rodlike molecules.

Figure 8 shows the average volume fraction of the rodlike chain fluids in the slit as a function of the bulk volume fraction at the separation of $H = 10\sigma$ and different head−head interactions of $\epsilon_{HH}^* = 3$, 5, 8, and 10. When the head−head interaction is equal to 3, the average volume fraction of the

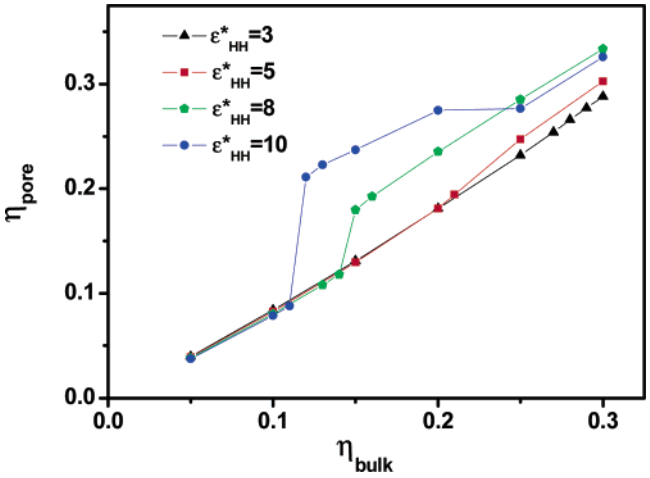

Figure 8. The average volume fraction of fluids in the slit as a function of the bulk volume fraction at $H = 10\sigma$ at different head−head interactions where the head−tail and tail−tail interactions are $\epsilon^*_{HT} = -1$, $\epsilon^*_{TT} = 1$, respectively (negative stands for the repulsion)

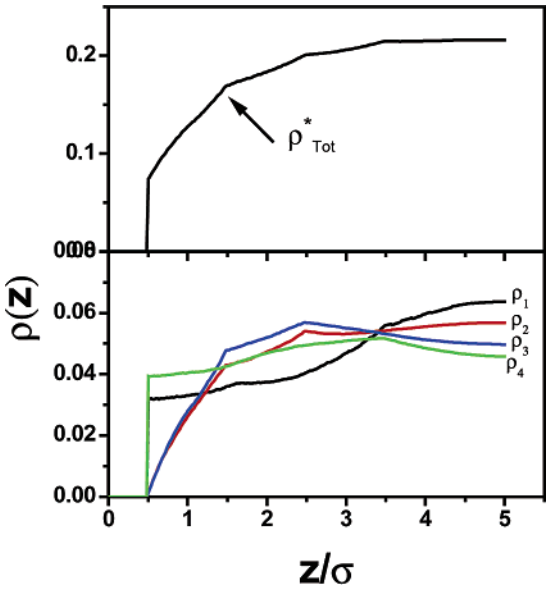

Figure 9. Local density (bottom panel) and total density (top panel) profiles of the rodlike molecule of chain length $M = 4$ at $\eta_{bulk} = 0.11$ in the slit of $H = 10\sigma$ where head−head interaction is $\epsilon^*_{HH} = 10$.

rodlike chain fluids in the slit increases with the bulk volume fraction linearly. However, when the head−head interaction has a strong attraction, i.e., $\epsilon^*_{HH} = 8$ and 10, suggesting that the rodlike molecule has a strong trend for self-assembly, the average volume fraction of the rodlike chain fluids in the slit shows an abrupt jump at the bulk volume fraction of $\eta_{bulk} = 0.12$. The abrupt jump corresponds to the first-order transition from the disorder to the order state, which has been discussed in previous publications for the flexible chains.[33,37] To further gain insight into the microscopic information corresponding to the jump, we present in Figures 9 and 10 the local density profiles at $\epsilon^*_{HH} = 10$ and the bulk volume fractions of $\eta_{bulk} = 0.11$ and 0.12, respectively. Obviously, the local density of the confined rodlike chain fluids at $\eta_{bulk} = 0.11$ indicates that the rodlike chain fluids are in the disorder state without any phase separation. Furthermore, the total density presents the strong depletion effect due to the loss of the configurational entropy, as shown in Figure 9. However, the local density of the confined rodlike chain fluids at $\eta_{bulk} = 0.12$ suggests that the rodlike molecules are orderly arranged in the slit. The head segments

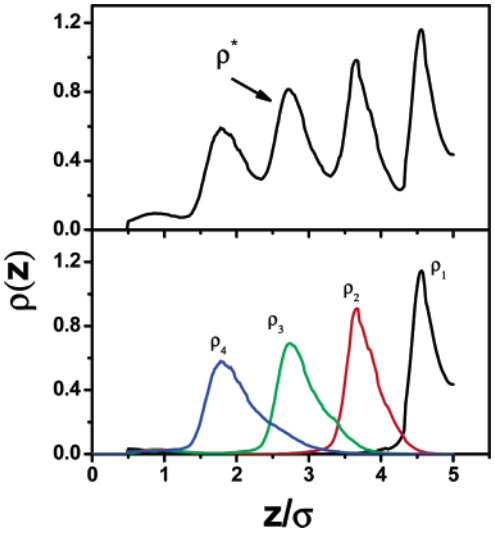

Figure 10. The conditions are the same as those for Figure 9 except $\eta_{bulk} = 0.12$.

self-assemble in the center of the slit, and all the rodlike molecules show the microscopic orientation perpendicular to the surfaces. Therefore, a thin film of lamellar structure is formed in the slit. Since the separation ($H = 10\sigma$) is larger than the thickness of the thin film, a small gap appears between the surface and the thin film. Because of the strong head−head interaction and the depletion effect caused by the small gap, the rodlike chain molecules cannot enter the small gap. Accordingly, in the range of $z < 1.5\sigma$, the density of the rodlike chain fluids is equal to zero approximately, as presented in Figure 10. For more information on the microscopic orientation of the rodlike molecules, we define the polar angle θ of the rod orientation as $\theta = \arccos(z_M - z_1/L)$, where L denotes the molecular length, and z_1 and z_M are the positions corresponding to the peaks of the local densities of two end segments, respectively. In the case studied, the calculated polar angle (i.e., the angle to the surface normal direction) is less than 10°, which is distinct evidence that the rodlike molecules orient basically perpendicular to the surface, although it is not in perfectly normal orientation. It is noted that the observed ordering structure is of uniaxial symmetry, i.e., perpendicular geometry. For the present DFT theory, it can only capture the uniaxial symmetry based on the microscopic information of the local segmental densities. As discussed earlier, due to the absence of molecular orientation distribution in the excess free energy, the DFT cannot capture the biaxial symmetry,[22] i.e., the structure parallel to the surface, from the local segment densities.

We can observe from Figure 8 that when the head−head interaction decreases from $\epsilon^*_{HH} = 10$ to 8, the bulk volume fraction corresponding to the jump increases from $\eta_{bulk} = 0.12$ to 0.15. That is to say, the critical bulk concentration for the self-assembly increases with the decrease of the head−head interaction. Figures 11 and 12 show the local density profiles of the rodlike chain fluids of $\epsilon^*_{HH} = 8$ in the slit of $H = 10\sigma$ at $\eta_{bulk} = 0.14$ and 0.15, respectively. Similar with Figure 9, the local density profiles at $\eta_{bulk} = 0.14$ shown in Figure 11 indicate that the rodlike chain fluids are still in the disorder state, while at $\eta_{bulk} = 0.15$, the rodlike chain fluids present an order lamellar structure in the slit, as shown in Figure 12. Compared with Figure 10, however, the part rodlike molecules enter the small gap between the surface and the thin film due to the decrease of the head−head interaction. For an intuitionistic understanding, we present in Figure 13 the schematic diagram for the order thin film formed by the rodlike molecules.

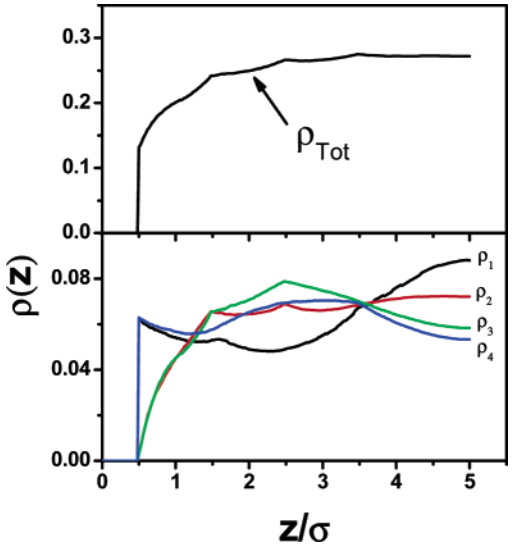

Figure 11. Local density (bottom panel) and total density (top panel) profiles of rodlike molecule of chain length $M = 4$ at $\eta_{bulk} = 0.14$ in the slit of $H = 10\sigma$ where head−head interaction is $\epsilon^*_{HH} = 8$.

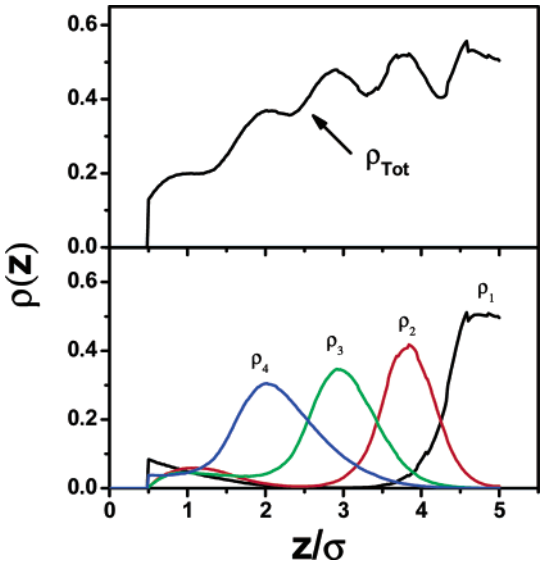

Figure 12. The conditions are the same asthose for Figure 11 except $\eta_{bulk} = 0.15$.

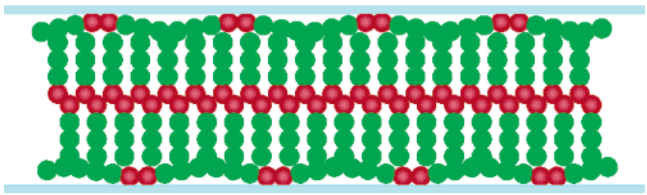

Figure 13. Schematic diagram for the lamellar thin film formed by the rodlike molecules perpendicular to the surface.

Apparently, in the above investigation, the separation between two neutral surfaces does not match the thickness of the thin film formed by the rodlike molecules. Therefore, we changed the separation to $H = 8\sigma$ to match the thickness of the thin film. Figure 14 shows the average volume fraction of rodlike chain fluids in the slit as a function of the bulk density at $H = 8\sigma$. Obviously, the behavior of the rodlike chain fluids in the slit is the same as that in Figure 8. In particular, our emphasis is placed on the structure of the thin film formed by the rodlike molecules. To compare with the behavior of the rodlike chain fluids in Figure 12, Figure 15 presents the local density profiles

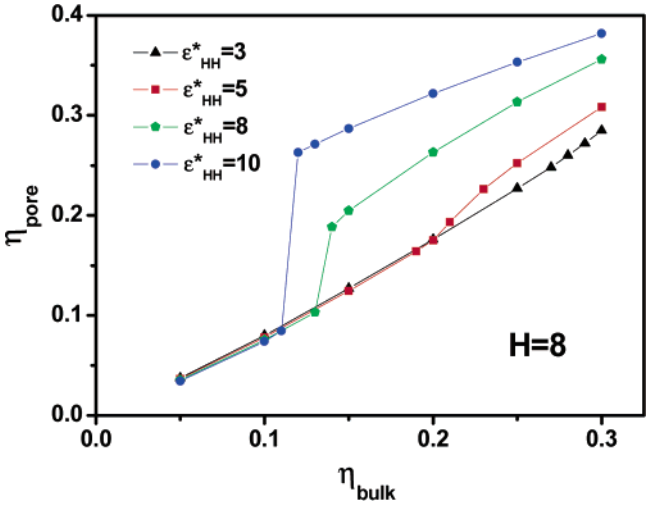

Figure 14. The average volume fraction of fluids in the slit as a function of the bulk volume fraction at $H = 8\sigma$ at different head−head interactions.

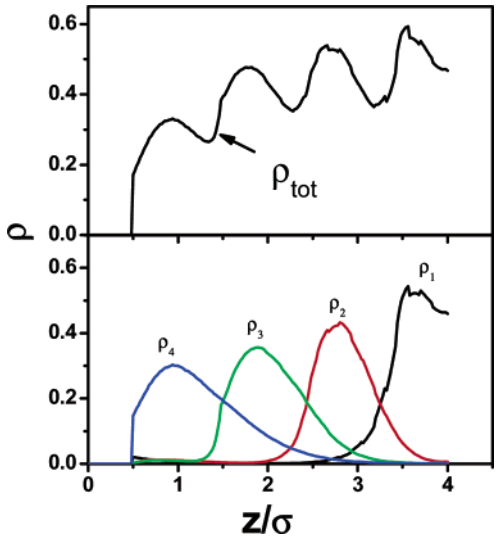

Figure 15. Local density (bottom panel) and total density (top panel) profiles of the rodlike molecule of chain length $M = 4$ at $\eta_{bulk} = 0.14$ in the slit of $H = 8\sigma$ where head−head interaction is $\epsilon^*_{HH} = 8$.

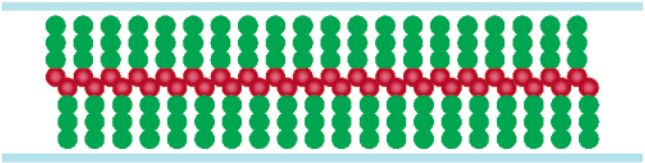

Figure 16. Schematic diagram for the self-assembly of rodlike molecules in the slit of $H = 8\sigma$.

of the rodlike chain fluids at the same conditions as that in Figure 12 except the separation of $H = 8\sigma$. The difference with Figure 12 is that the lamellar thin film is closely near the surfaces. That is to say, the lamellar structure exhibits in the slit perfectly. Figure 16 presents the schematic diagram of the lamellar thin film formed by rodlike molecules perpendicular to the surface.

5. Conclusions

The hybrid density functional approach was used to investigate the microstructure and self-assembly of inhomogeneous rodlike chain fluids confined between two neutral surfaces. In the calculation, the single-chain simulation was adopted for the

calculation of the ideal-gas part of Helmholtz energy, and the DFT approach was used for the evaluation of the excess Helmholtz energy. The DFT approach includes a modified fundamental measure theory for the excluded-volume effect, the first order thermodynamics perturbation theory for chain connectivity, and a mean field approximation for the van der Waals attraction. For athermal systems, we found that the rodlike chain fluids present the smaller partitioning coefficient compared to the flexible chain systems, suggesting that the rodlike molecules are difficult to enter the slit. The longer the rodlike molecule, the more difficult to enter the slit. For thermal systems, the lamellar thin films formed by the rodlike molecules perpendicular to the neutral surface are observed. When the head−head interaction is very strong, the lamellar thin film is abruptly formed from the disorder state with the increase of the bulk concentration. Furthermore, the critical bulk concentration for the self-assembly of the rodlike chain fluids in the slit increases with the decrease of the head−head interaction.

Acknowledgment. This work is supported by the National Natural Science Foundation of China (20646001) and the Excellent Talent Fund of Beijing University of Chemical Technology.

References and Notes

(1) Onsager, L. *Ann. N.Y. Acad. Sci* **1949**, *51*, 627.
(2) Cuetos, A.; Martinez-Haya, B.; Rull, L. F.; Lago, S. *J. Chem. Phys.* **2002**, *117*, 2934.
(3) Koenderink, G. H.; Vliegenthart, G. A.; Kluijtmans, S. G.; van Blaaderen, A.; Philipse, A. P.; Lekkerkerker, H. N. W. *Langmuir* **1999**, *15*, 4693.
(4) Bolhuis, P.; Frenkel, D. *J. Chem. Phys.* **1997**, *106*, 666.
(5) Bolhuis, P. G.; Stroobants, A.; Frenkel, D.; Lekkerkerker, H. N. W. *J. Chem. Phys.* **1997**, *107*, 1551.
(6) McBride, C.; Vega, C.; MacDowell, L. G. *Phys. Rev. E* **2001**, *6401*.
(7) Schmidt, M.; Dijkstra, M. *J. Chem. Phys.* **2004**, *121*, 12067.
(8) Bryk, P. *Phys. Rev. E* **2003**, *68*, 062501.
(9) Esztermann, A.; Reich, H.; Schmidt, M. *Phys. Rev. E* **2006**, *73*, 011409.
(10) Schmidt, M. *Phys. Rev. E* **2001**, *63*, 050201.
(11) Adams, M.; Dogic, Z.; Keller, S. L.; Fraden, S. *Nature* **1998**, *393*, 349.
(12) Chen, Y. L.; Schweizer, K. S. *J. Chem. Phys.* **2002**, *117*, 1351.
(13) Cao, D. P.; Wu, J. Z. *Langmuir* **2005**, *21*, 9786.
(14) Velasco, E.; Mederos, L.; Sullivan, D. E. *Phys. Rev. E* **2000**, *62*, 3708.
(15) de las Heras, D.; Mederos, L.; Velasco, E. *Phys. Rev. E* **2003**, *68*, 031709.
(16) Tarazona, P. *Phys. Rev. Lett.* **2000**, *84*, 694.
(17) Yu, Y. X.; Wu, J. Z. *J. Chem. Phys.* **2002**, *117*, 2368.
(18) Vega, C.; McBride, C.; MacDowell, L. G. *J. Chem. Phys.* **2001**, *115*, 4203.
(19) Blas, F. J.; Sanz, E.; Vega, C.; Galindo, A. *J. Chem. Phys.* **2003**, *119*, 10958.
(20) Vega, C.; McBride, C. *Phys. Rev. E* **2002**, *65*, 052501.
(21) Cao, D. P.; Wu, J. Z. *J. Chem. Phys.* **2006**, *124*, 164904.
(22) van Roij, R.; Dijkstra, M.; Evans, R. *J. Chem. Phys.* **2000**, *113*, 7689.
(23) Harnau, L.; Penna, F.; Dietrich, S. *Phys. Rev. E* **2004**, *70*, 021505.
(24) Bryk, P.; Bucior, K.; Sokolowski, S.; Zukocinski, G. *J. Phys. Chem. B* **2005**, *109*, 2977.
(25) Bryk, P.; Pizio, O.; Sokolowski, S. *J. Chem. Phys.* **2005**, *122*.
(26) Bryk, P.; Sokolowski, S. *J. Chem. Phys.* **2004**, *121*, 11314.
(27) Kierlik, E.; Rosinberg, M. L. *J. Chem. Phys.* **1992**, *97*, 9222.
(28) Jaffer, K. M.; Opps, S. B.; Sullivan, D. E. *J. Chem. Phys.* **1999**, *110*, 11630.
(29) Jaffer, K. M.; Opps, S. B.; Sullivan, D. E.; Nickel, B. G.; Mederos, L. *J. Chem. Phys.* **2001**, *114*, 3314.
(30) Yu, Y. X.; Wu, J. Z. *J. Chem. Phys.* **2002**, *117*, 10156.
(31) Roth, R.; Evans, R.; Lang, A.; Kahl, G. *J. Phys.: Condens. Matter* **2002**, *14*, 12063.
(32) Bryk, P.; Sokolowski, S. *J. Chem. Phys.* **2004**, *120*, 8299.
(33) Li, Z. D.; Cao, D. P.; Wu, J. Z. *J. Chem. Phys.* **2005**, *122*, 174708.
(34) Yu, Y. X.; Wu, J. Z. *J. Chem. Phys.* **2003**, *118*, 3835.
(35) Cao, D. P.; Wu, J. Z. *Langmuir* **2006**, *22*, 2712.
(36) Li, Z. D.; Cao, D. P.; Wu, J. Z. *J. Chem. Phys.* **2005**, *122*, 224701.
(37) Malijevsky, A.; Bryk, P.; Sokolowski, S. *Phys. Rev. E* **2005**, *72*, 032801.
(38) Cao, D. P.; Wu, J. Z. *Macromolecules* **2005**, *38*, 971.
(39) Cao, D. P.; Wu, J. Z. *J. Chem. Phys.* **2004**, *121*, 4210.
(40) Cao, D. P.; Wu, J. Z. *J. Chem. Phys.* **2005**, *122*, 194703.
(41) Rosenfeld, Y. *J. Phys.: Condens. Matter* **2002**, *14*, 9141.
(42) Rosenfeld, Y. *Phys. Rev. Lett.* **1989**, *63*, 980.
(43) Yethiraj, A.; Woodward, C. E. *J. Chem. Phys.* **1995**, *102*, 5499.